PERGAMON

International Journal of Heat and Mass Transfer 41 (1998) 4183–4194

International Journal of HEAT and MASS TRANSFER

Evaporation heat transfer and pressure drop of refrigerant R-134a in a small pipe

Yi-Yie Yan, Tsing-Fa Lin*

Department of Mechanical Engineering, National Chiao Tung University, Hsinchu 30049, Taiwan, R.O.C.

Received 10 October 1997; in final form 20 March 1998

Abstract

An experiment was carried out to investigate the characteristics of the evaporation heat transfer and pressure drop for refrigerant R-134a flowing in a horizontal small circular pipe having an inside diameter of 2.0 mm. The data are useful in designing more compact and effective evaporators for various refrigeration and air conditioning systems. The effects of the imposed wall heat flux, mass flux, vapor quality and saturation temperature of R-134a on the measured evaporation heat transfer and pressure drop were examined in detail. When compared with the data for larger pipes ($D_i \geqslant 8.0$ mm) reported in the literature, the evaporation heat transfer coefficient for the small pipe considered here is about 30–80% higher for most situations. Moreover, we noted that in the small pipe the evaporation heat transfer coefficient is higher at a higher imposed wall heat flux except in the high vapor quality region, at a higher saturation temperature, and at a higher mass flux when the imposed heat flux is low. In addition, the measured pressure drop is higher for increases in the mass flux and imposed wall heat flux. Based on the present data, empirical correlations were proposed for the evaporation heat transfer coefficients and friction factors. © 1998 Elsevier Science Ltd. All rights reserved.

Nomenclature

A heat transfer area [m^2]
B_0 boiling number $= q''_w/(i_{fg}G)$
C_c coefficient of contraction, equation (11)
C_0 convection number $= (1-X_m/X_m)^{0.8}\,(\rho_g/\rho_1)^{0.5}$
$C_1 \sim C_4$ constants in equation (17)
$C_{m,1} \sim C_{m,3}$ constants in equation (21)
c_p specific heat [J kg^{-1} °C]
D_i pipe inside diameter [m]
Fr_{lo} Froude number based on total flow assumed as liquid $= G^2/(\rho_1{}^2 g D_i)$
f friction factor
G mass flux [kg m^{-2} s^{-1}]
g acceleration due to gravity [m s^{-2}]
h heat transfer coefficient [W m^{-2}°C] i_{fg} enthalpy of vaporization [J kg^{-1}]
k conductivity
L length of the pipe tested [m]
Nu Nusselt number
P pressure [MPa]
Pr Prandtl number
Q heat transfer rate [W]
q''_w imposed wall heat flux [W m^{-2}]
Re Reynolds number, dimensionless
Re_{eq} equivalent all liquid Reynolds number, equation (23)
T temperature [K]
T_c critical temperature [K]
T_R reduced temperature $= T/T_c$
v specific volume [m^3 kg^{-1}]
W mass flow rate [kg s^{-1}]
X vapor quality.

Greek symbols
α void fraction, dimensionless
μ viscosity [N s^{-1} m^{-2}]
ρ density [kg m^{-3}]
σ contraction ratio.

Subscripts
a acceleration
exp experiment

* Corresponding author.

0017–9310/98 $19.00 © 1998 Elsevier Science Ltd. All rights reserved
PII: S0017–9310(98)00127–6

f friction
fg difference between liquid phase and vapor phase
g vapor phase
h heater
i, o at inlet and exit of test section
lat, sens latent and sensible heats
l liquid phase/assume all the flow as liquid
m average value for the two phase mixture or between the inlet and exit
p pre-evaporator
r refrigerant
sat saturated
tp two-phase
w water
wall inner wall of the small pipes.

1. Introduction

To avoid the destruction of the ozone layer in the outer atmosphere around the earth, various non-CFC refrigerants were recently introduced and then used in different air conditioning and refrigeration systems. Among these refrigerants, HFC refrigerant R-134a is currently used in many home and automobile air conditions. In view of energy conservation and space saving, the design of more efficient and compact air conditioners is relatively important. Recently very small evaporator and condenser tubes of about 2 mm in diameter were considered in the air conditioners to achieve the above goals. It is well known that in the very small tubes the capillary effects are prominent. Hence the evaporating or condensing refrigerant flow is annular or plug, instead of being stratified, and the associated heat transfer is expected to be better. In addition, the air side convection heat transfer coefficient over smaller tubes is higher. Although a considerable amount of data on the boiling and condensation of R-134a in larger tubes with their diameters larger than 6 mm has been recently reported in literature, very little is known of the small tubes. In the present study an experiment is conducted to measure the evaporation heat transfer coefficient and pressure drop in a R-134a flow through a heated small pipe having an inside diameter of 2.0 mm.

An update comprehensive review of the literature on nucleate pool boiling and intube flow boiling of new refrigerants was given by Thome [1]. The pipe diameter tested in the works cited in this review ranges from 6.35 to 21.2 mm. This is in accordance with the fact that the pipes used in the majority of current air conditioning and refrigeration systems have their diameters larger than 6.35 mm. In the following the relevant literature on the present study is briefly reviewed.

Eckels and Pate [2] measured evaporation heat transfer coefficients for R-134a and R-12 in a horizontal, smooth tube with an inner diameter of 8.0 mm. They noted that for similar mass fluxes the evaporation heat transfer coefficient for R-134a exceeded that for R-12 by about 35–45%. Besides, the heat transfer coefficient increases with the saturation temperature and mass flux. In a continuing study [3] they further showed that the R-134a evaporation heat transfer coefficient for a micro-fin tube was 50–150% more than that for a smooth tube. The associated pressure drop penalty factor resulting from the micro-fin surface was usually less than the heat transfer enhancement factor. Experiments from Torikoshi and Ebisu [4], in a tube with an inner diameter of 8.7 mm, indicated that the evaporation heat transfer coefficient for R-134a was about 15% lower than that for R-22, while the pressure drop for R-134a was about 63% larger than that for R-22. But a different trend was found by Hambraeus [5] in larger smooth, horizontal tubes in that the R-134a evaporation heat transfer is better than that for R-22. Moreover, the effect of the oil, in the refrigerant, on the evaporation heat transfer depends significantly on the imposed heat flux. In an annular flow Wattlet et al. [6] noted that the evaporation heat transfer coefficient for R-134a was on average 25% higher than that for R-12 in a horizontal, smooth copper tube of 10.21 mm in diameter. The experiments for flow boiling of R-134a and R-12 in an annular passage with an enhanced surface from Sami et al. [7] showed two heat transfer regions, a nucleate boiling region and a forced convective region. Observation of flow boiling of R-134a in a micro-fin tube by Singh et al. [8] indicated that at the mass flux of 100 $kg\,m^{-2}\,s^{-1}$ a transition from a stratified to annular flow occurred. This corresponds to the all flow liquid Froude number of 0.058. Recently Liu [9] noted that in an axially grooved tube the evaporation heat transfer coefficient of R-134a is close to that of R-22 for the mass flux below 270 $kg\,m^{-2}\,s^{-1}$. Beyond that the R-134a has a lower heat transfer coefficient.

The above literature review clearly indicates that the heat transfer and pressure drop data for the evaporation of R-134a in small tubes having diameter smaller than 4 mm are not available. In this study, the characteristics of evaporation heat transfer and pressure drop for refrigerant R-134a flowing in a small pipe of 2 mm inside diameter were explored experimentally. The measured heat transfer coefficient for this small pipe was compared with that for larger pipes. Moreover, correlation equations for the heat transfer coefficient and pressure drop for this small pipe were proposed.

2. Experimental apparatus and procedure

The experimental apparatus established in the present study schematically shown in Fig. 1 consists of three main loops, a DC power supply and a data acquisition system. More specifically, the three main loops include a refrigerant loop, a water loop and a water–glycol loop. Refriger-

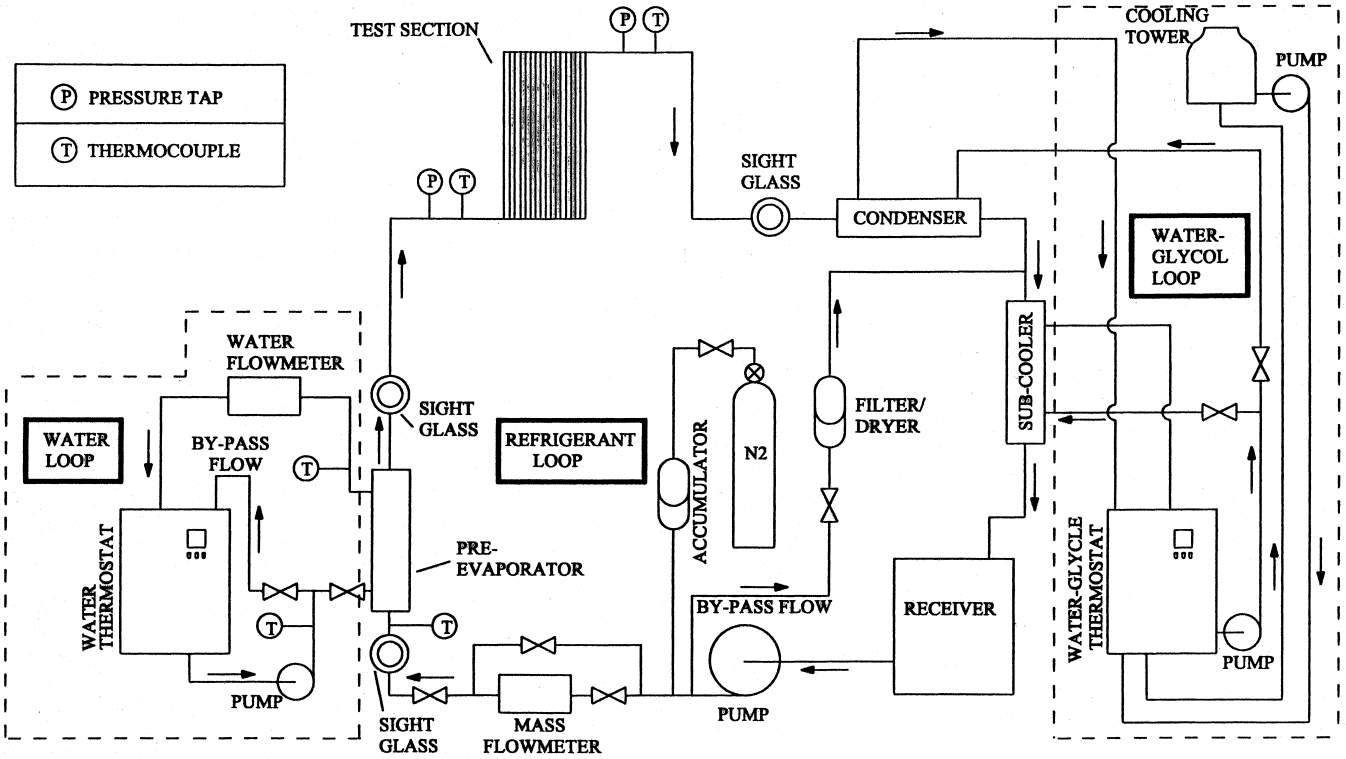

Fig. 1. Schematic diagram of the experimental system.

ant R-134a is circulated in the refrigerant loop. We need to control the temperature and flow rate in the water and water–glycol loops to obtain the preset inlet vapor quality and pressure in the test section in the refrigerant loop. Meanwhile, the current of the DC power supply was adjusted to achieve the required heat flux imposed on the small tubes in the test section.

2.1. Refrigerant loop

The refrigerant loop contains a refrigerant pump, an accumulator, a mass flow-meter, a pre-evaporator, a test section, a condenser, a sub-cooler, a receiver, a filter/dryer and three sight glasses. The refrigerant pump is driven by a DC motor which is in turn controlled by a variable DC output motor controller. The liquid flow rate of R-134a was varied by a rotational DC motor through changing the DC current. The refrigerant flow rate can be further adjusted by opening the by-pass valve. In the loop the accumulator was used to dampen the fluctuations of the flow rate and pressure. The refrigerant flow rate was measured by a mass flow meter with an accuracy of $\pm 1\%$. The pre-evaporator was used to evaporate the refrigerant R-134a to a specified vapor quality at the test section inlet by receiving heat from the hot water in the water loop. Note that the amount of heat transfer from the hot water to the refrigerant in the pre-evaporator is calculated from the energy balance in the water flow. Meanwhile, a condenser and a sub-cooler were used to condense the refrigerant vapor from the test section by the cold water–glycol loop. The pressure of the refrigerant loop can be controlled by varying the temperature and flow rate of the water–glycol in the condenser,. After condensing, the liquid refrigerant flows back to the receiver.

2.2. Test section

Because the pipes tested were relatively small, the refrigerant flow rates in them were very small and direct measurement of heat transfer and pressure drop in the pipe is difficult and is subject to large error. Thus 28 small pipes, each having the same diameter and length, were put together to form the test section, as shown in Fig. 2(a). Each small pipe has an inside diameter of 2.0 mm, outside diameter of 3.0 mm and length of 0.2 m. Specifically, these 28 pipes were placed together side by side forming a plane bundle. At the middle axial station of the pipes 10 thermocouples were soldered on the outer surface of the pipes. These thermocouples are soldered on 10 selected pipes at circumferential positions of 45° from the top of the pipe or from the bottom of the pipe, as shown in Fig. 2(b). Two copper plates of 5 mm thick were soldered on the upper and lower sides of the pipe bundle. The width of each copper plate was the same as the pipe bundle but it was only 0.1 m long. Obviously small crevices exist between the pipe outside surface and copper plates. Therefore the thermocouple wires were placed along these cervices. Due to the good thermal contact of the copper plates and the pipes, there is no need to fill the crevices with grease. Instead, the crevices provide the space for the thermocouple wires leading to the data logger. Each copper plate is in turn covered with a stainless steel plate (SS304) 0.07 mm thick. Acting as a heater, the stainless plate was connected to a 1.8 kW DC power supply. Adhesive plaster was put into the space between the stainless steel and copper plates to prevent leakage of electric current to the copper plates The power input to the heaters was measured by a power meter with an accuracy of $\pm 0.5\%$. To reduce the heat loss from the heaters, the whole test section was wrapped with 0.1 m thick polyethylene. Care was taken to design the inlet and outlet of the connection pipe to the pipe bank so that the R-134a flow rate in each small pipe was nearly the same. The pressure and pressure drop at and across the pipe inlet and exit were measured by the pressure transducers having an accuracy of $\pm 1\%$.

2.3. Water loop for pre-evaporator

A double pipe heat exchanger having a heat transfer area of 0.12 m^2 was used as the pre-evaporator. The liquid R-134a flow in the inner pipe was heated to a specific vapor quality by the hot water flowing in the outer pipe. The pre-evaporator and the connection pipe between the test section and the pre-evaporator were thermally well insulated with 0.06 m thick polyethylene. The water loop designed for the pre-evaporator consists of a 125-l hot water container with three 2.0 kW heaters in it and a 0.5 hp water pump to drive the hot water at specified temperature and flow rate to the pre-evaporator. Similarly, a by-pass valve is also used to adjust the flow rate. The water flowmeter has an accuracy of $\pm 0.5\%$.

2.4. Water–glycol loop

The water–glycol loop designed for condensing the R-134a vapor contains a 125-l container with a water cooled refrigeration system. The cooling capacity is 2 kW for the water–glycol at -20°C. The cold water–glycol at a specified flow rate is driven by a 0.5 hp pump to the condenser as well as to the sub-cooler. A by-pass loop is also provided to adjust the flow rate.

2.5. Data acquisition

The data acquisition system includes a recorder, a 24V-3A power supply and a controller. The recorder was used to record the temperature and voltage data. The water flowmeter and differential pressure transducer need a 24 V power supply as a driver to output an electric current of 4–20 mA. The IEEE488 interface was used to connect

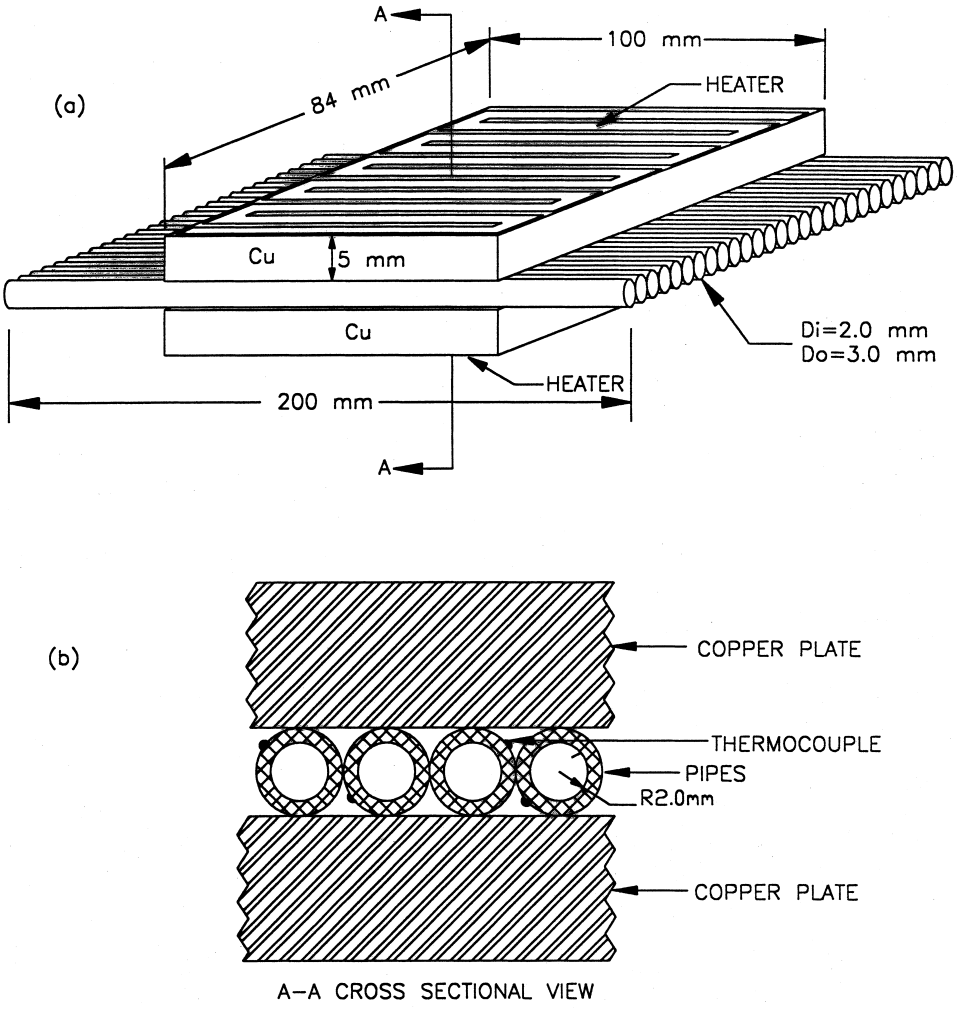

Fig. 2. (a) Test section of the small pipes and (b) locations of the thermocouples.

the controller and the recorder, allowing the measured data to transmit from the recorder to the controller and then analyzed by the computer immediately.

2.6. Experimental procedures

In the test, the R-134a pressure at the test section inlet was first maintained at a specified level by adjusting the water–glycol temperature and its flow rate. Then, the temperature and flow rate of the hot water loop for the pre-evaporator was adjusted to keep the vapor quality of R-134a at the test section inlet at the desired value. Finally, the heat transfer rate from the heaters to R-134a in the refrigerant loop was adjusted by changing the electric current delivered from the DC power supply. By measuring the current and voltage drop across the heaters, we could calculate the amount of the heat transfer to the refrigerant.

3. Data reduction

An analysis is needed to calculate the evaporation heat transfer coefficient and friction factor from the experimental data. This data reduction process is described in the following.

3.1. Single phase heat transfer

Before measuring the evaporation heat transfer and pressure drop, a single phase heat transfer test was conducted first to check the energy balance in the test section. The results indicated that the energy balance between the heater and the refrigerant was within 2% for all runs. This insures the heat loss from the test section being rather small and the test section being appropriate for our measurement.

3.2. Two-phase evaporation heat transfer

The vapor quality of R-134a at the test section inlet was evaluated from the energy balance for the pre-evaporator. Based on the temperature drop on the water side the total heat transfer rate from the water to the refrigerant can be calculated from

$$Q_{w,p} = W_{w,p} c_{p,w} (T_{w,p,i} - T_{w,p,o}) \quad (1)$$

This heat transfer to the refrigerant causes its temperature to rise to the saturated value (a sensible heat transfer process) and the refrigerant to evaporate (a latent heat transfer process). Thus,

$$Q_{w,p} = Q_{sens} + Q_{lat} \quad (2)$$

where

$$Q_{sens} = W_r c_{p,r} (T_{r,p,o} - T_{r,p,i}) \quad (3)$$

$$Q_{lat} = W_r i_{fg} X_{p,o}. \quad (4)$$

The above equations can be combined to evaluate the refrigerant quality at the exit of the pre-evaporator, that is considered to be the same as the vapor quality of the refrigerant entering the test section. Specifically,

$$X_i = X_{p,o} = \frac{1}{i_{fg}} \left[\frac{Q_{w,p}}{W_r} - c_{p,r} (T_{r,p,o} - T_{r,p,i}) \right]. \quad (5)$$

The total change of the refrigerant vapor quality in the test section was then deduced from the imposed heat input to the refrigerant in the test section:

$$\Delta X = \frac{Q_h}{i_{fg} W_r} \quad (6)$$

where Q_h is the total heat generation rate due to resistance heating in the heaters. Finally, the heat transfer coefficient for the evaporation of R-134a was determined from the definition

$$h \equiv \frac{Q_h}{A(T_{wall} - T_r)} \quad (7)$$

where T_{wall} is the average of the measured pipe wall temperature at the detected locations and T_r is the mean refrigerant temperature which is, in turn, estimated from the measured refrigerant temperatures at the test section inlet and exit,

$$T_r = \frac{(T_{r,i} + T_{r,o})}{2} \quad (8)$$

3.3. Two phase friction factor

To evaluate the friction factor associated with the R-134a evaporation, the friction pressure drop ΔP_f was first calculated by subtracting the acceleration pressure drop ΔP_a and the pressure losses at the test section inlet and exit ΔP_i and ΔP_o from the measured total pressure drop ΔP_{exp}

$$\Delta P_f = \Delta P_{exp} - \Delta P_a - \Delta P_i + \Delta P_o. \quad (9)$$

Note that the acceleration pressure drop was estimated by the homogeneous model for two phase gas–liquid flow [10], that is

$$\Delta P_a = G^2 v_{fg} \Delta X. \quad (10)$$

The two phase pressure drops in the sudden contraction and expansion were estimated by the separated flow model, as recommended by Collier [10], and the results are

$$\Delta P_i = \left(\frac{G}{C_c}\right)^2 (1 - C_c) \left\{ \frac{(1 + C_c)[X_m^3 v_g^2/\alpha^2 + (1 - X_m)^3 v_l^2/(1-\alpha)^2]}{2[X_m v_g + (1 - X_m) v_l]} - C_c \left[\frac{X_m^2 v_g}{\alpha} + \frac{(1 - X_m)^2 v_g}{(1-\alpha)} \right] \right\} \quad (11)$$

$$\Delta P_o = G^2 \sigma (1 - \sigma) v_l \left[\frac{(1 - X_m)^2}{(1-\alpha)} + \left(\frac{v_g}{v_l}\right) \frac{X_m^2}{\alpha} \right] \quad (12)$$

where C_c in the above equation is called 'coefficient of contraction' and is a function of the contraction ratio σ. The void fraction α in the above equation was correlated by

$$\alpha = \frac{1}{1 + \left(\frac{1 - X_m}{X_m}\right)\left(\frac{\rho_g}{\rho_l}\right)^{2/3}}. \quad (13)$$

Based on the above estimation the acceleration pressure drop and the pressure losses at the test section inlet and exit are rather small and the friction pressure drop ranges from 95 to 98% of the total pressure drop. According to the definition

$$f_{tp} \equiv -\frac{\Delta P_f D_i}{2 G^2 v_m L} \quad (14)$$

the friction factor for the evaporation of R-134a in the small pipe was obtained, where v_m is the specific volume of the vapor-liquid mixture when they are homogeneously mixed and is given as

$$v_m = [X_m v_g + (1 - X_m) v_l] = [v_l + X_m v_{fg}]. \quad (15)$$

3.4. Uncertainty analysis

The uncertainties of the experimental results was analyzed by the procedures proposed by Kline and McClintock [12]. The detailed results from the present uncertainty analysis for the experiments conducted here are summarized in Table 1.

4. Results and discussion

To check the suitability of the above experimental system for the present measurement, the single phase liquid R-134a heat transfer data were measured first and com-

Table 1
Parameters and estimated uncertainties

Parameter	Uncertainty
Length, width and thickness (m)	±0.5%
Area (m^2)	±1%
Temperature, T	±0.1°C
ΔT	±0.14°C
Pressure, P	±0.001 MPa
Measured pressure drop, ΔP_{exp}	±40 Pa
Water flow rate in pre-evaporator, $W_{w,p}$	±2%
Mass flux of refrigerant, G	±2%
Heat transfer rate of test section, Q_h	±0.5%
Heat transfer of pre-evaporator, $Q_{w,p}$	±4%
Vapor quality, X	±0.03
Single liquid phase heat transfer coefficient, h	±6%
R-134a evaporation heat transfer coefficient, h_r	±6%
Two-phase friction factor, f_{tp}	±10%

pared with the well known correlation from Dittus–Boelter [5] in Fig.3. The correlation is

$$Nu = 0.023 Re^{0.8} Pr^{0.4} \left(\frac{\mu_m}{\mu_{wall}}\right)^{0.14}. \quad (16)$$

The comparison indicates that our experimental results are in good agreement with the Dittus–Boelter correlation for the mass flux G above 200 kg m^{-2} s^{-1}. At $G < 200$ kg m^{-2} s^{-1} the experimental data depart significantly from those calculated by the Dittus–Boelter correlation. This results from the fact that at $G < 200$ kg m^{-2} s^{-1} the corresponding Reynolds number in the small pipe studied here is below 2000 and the flow is laminar. Through the above comparison the present experimental design is considered to be suitable for the present measurement of two phase evaporation heat transfer and pressure drop. After this single phase test we started to investigate the effects of various parameters, namely, the mass flux, heat flux and saturated temperature on the heat transfer and pressure drop in the two-phase R-134a flow. In what follows only a small sample of the results obtained is presented to illustrate these effects.

4.1. Two-phase evaporation heat transfer

In the present investigation of the R-134a evaporation in the small pipe the R-134a mass flux was varied from 50 to 200 kg m^{-2} s^{-1}, imposed heat flux from 5 to 20 kW m^{-2} and saturation temperature from 5 to 31°C. The measured heat transfer coefficient and pressure drop are to be presented in terms of their variations with the average vapor quality in the test section. Since the pipe is short, the vapor quality change in the test section is small, $\Delta X < 0.01$.

The effects of the imposed wall heat flux on the R-134a evaporation heat transfer are examined first. Figure 4 presents the variations of our measured heat transfer coefficient with the average vapor quality X_m at four different heat flux levels for $T_{sat} = 5$ and 31°C at $G = 100$ kg m^{-2} s^{-1}. The results indicate that at a given vapor quality the heat transfer coefficient is higher for a higher wall heat flux except at a higher vapor quality with $X_m > 0.58$ for $T_{sat} = 5$°C and with $X_m > 0.8$ for

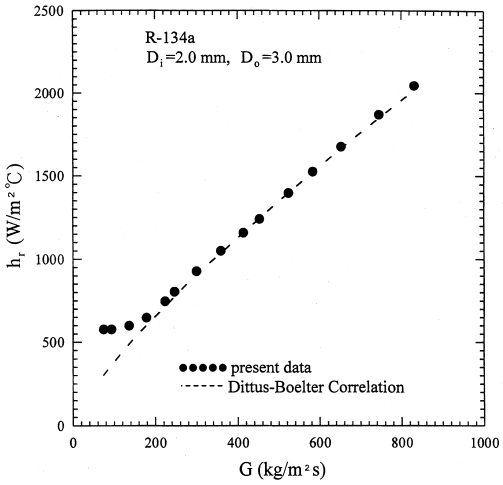

Fig. 3. Comparison of the present data for the liquid phase heat transfer coefficient with the Dittus–Boelter.

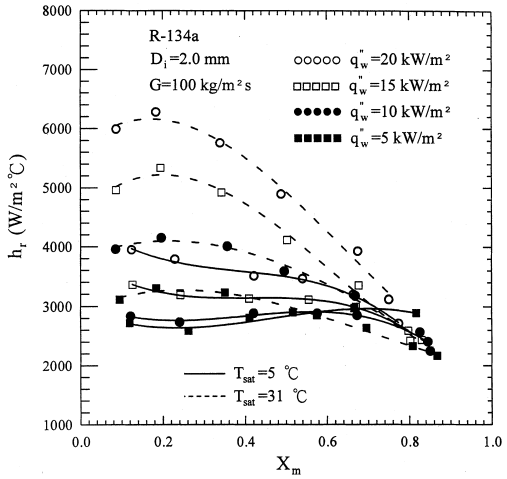

Fig. 4. Variations of the evaporation heat transfer coefficient with the imposed wall heat flux at different mean vapor quality for $T_{sat} = 5$ and 31°C and $G = 100$ kg m^{-2} s^{-1}.

$T_{sat} = 31°C$. Moreover, at $T_{sat} = 5°C$ the increase of the heat transfer coefficient with the heat flux is larger at a lower X_m. But at $T_{sat} = 31°C$ a maximum increase in the heat transfer with the heat flux appears at $X_m \approx 0.2$. Moreover, it is noted that at a given q''_w for $T_{sat} = 5°C$ the heat transfer coefficient decreases with the increase in the vapor quality when X_m is low. As X_m exceeds certain critical values, the trend reverses with the heat transfer coefficient being higher at a higher X_m for $q''_w \leqslant 15$ kW m^{-2}. At an even higher vapor quality the heat transfer coefficient again decreases with the increase in the vapor quality for $q''_w \geqslant 10$ kW m^{-2}. Thus, the variation of the heat transfer coefficient with the vapor quality is non-monotonic. However, for $T_{sat} = 31°C$ the change of h_r with X_m is somewhat different. Specifically, h_r increases with X_m at a low vapor quality, but a reverse trend is the case at a high vapor quality. Thus, there exists a peak h_r at a certain X_m for each q''_w. It should be mentioned that for larger pipes with $D_i \geqslant 6.35$ mm the imposed wall heat flux exhibits noticeable effects on the evaporation heat transfer only at a low vapor quality [13, 14], $X_m < 0.3$.

The evaporation heat transfer affected by the wall heat flux is further illustrated by examining the results in Fig. 5 for a higher mass flux, $G = 200$ kg m^{-2} s^{-1}. Note that at this higher mass flux a rise in the wall heat flux also causes a significant increase in the evaporation heat transfer in the region of low vapor quality for $X_m < 0.5$. It is important to note that at the high vapor quality with $X_m > 0.72$ the heat transfer coefficient for $q''_w = 5$ kW m^{-2} is much higher than that for the higher wall heat flux with $q''_w = 10$, 15 and 20 kW m^{-2}. This is attributed to the fact that at a high vapor quality the pipe wall may become partially dry when the wall heat flux is high enough. Obviously, the evaporation heat transfer deteriorates on the partially dry wall. For the case at the low heat flux $q''_w = 5$ kW m^{-2} the wall remains wet even at a high vapor quality. Moreover, at this vapor quality the vapor velocity is high and the convective evaporation is rather strong. Thus h_r increases with X_m for the entire range of the vapor quality for $q''_w = 5$ kW m^{-2}.

Next, the effects of the saturated temperature of the refrigerant on the evaporation heat transfer are exemplified in Fig. 6 for two different wall heat fluxes for the mass flux of 100 kg m^{-2} s^{-1}. Note that at the low imposed heat flux level of 5 kW m^{-2} the evaporation heat transfer is much more effective at the low saturated temperature of 15°C in the high vapor quality region with $X_m > 0.65$. While at the high heat flux level of 15 kW m^{-2} and in the low vapor quality region with $X_m < 0.5$ the trend is completely the reverse with the evaporation heat transfer at the high T_{sat} of 31°C dominating over that at $T_{sat} = 15°C$. This is due to the lower latent heat of vaporization of the higher saturation temperature and the bubble generation rate is higher at a low vapor quality. Thus, at a high q''_w the rise in the vaporization rate of R-134a in the low quality region for a higher T_{sat} overwhelms the reduction in the latent heat of vaporization and a higher evaporation heat transfer coefficient results. But in the high vapor quality region and at high q''_w and T_{sat} the pipe wall tends to become dry causing a sharp reduction in the heat transfer coefficient.

Then, how the refrigerant mass flux affects the evaporation heat transfer is presented in Figs 7 and 8 for two different imposed wall heat fluxes. The results in Fig. 7 for $q''_w = 5$ kW m^{-2} indicate that at a high vapor quality $X_m > 0.43$ the evaporation heat transfer coefficient rises with the mass flux. But at a lower vapor quality ($X_m < 0.4$) h_r for $G = 200$ kg m^{-2} s^{-1} can be below that

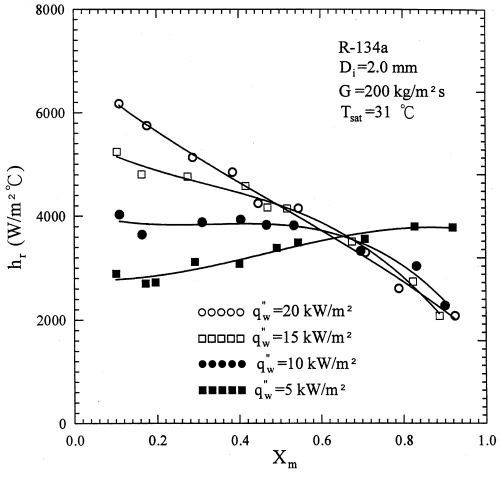

Fig. 5. Variations of the evaporation heat transfer coefficient with the imposed wall heat flux at different mean vapor quality for $T_{sat} = 31°C$ and $G = 200$ kg m^{-2} s^{-1}.

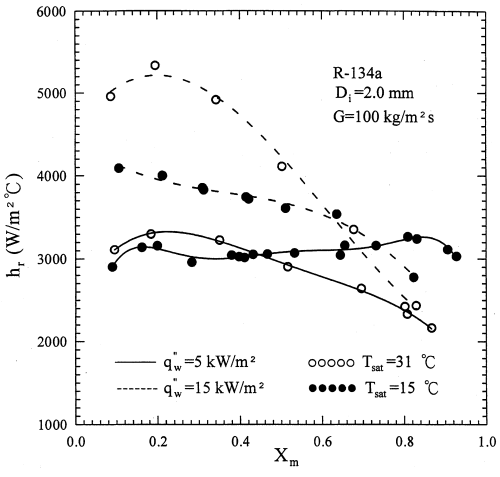

Fig. 6. Effects of the refrigerant saturated temperature on the evaporation heat transfer at two different wall heat fluxes for $G = 100$ kg m^{-2} s^{-1}.

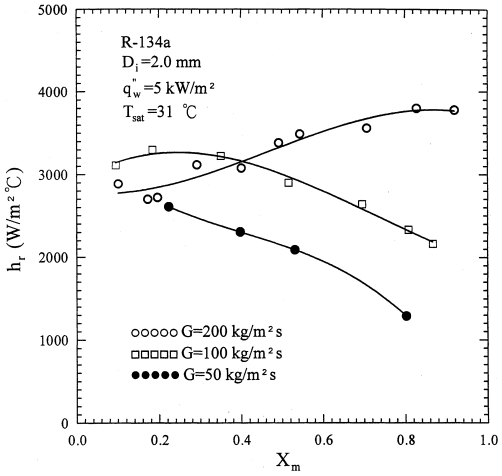

Fig. 7. Variations of the evaporation heat transfer coefficient with the mean flux at $T_{sat} = 31^{\circ}C$ and $q''_w = 5$ kW m^{-2}.

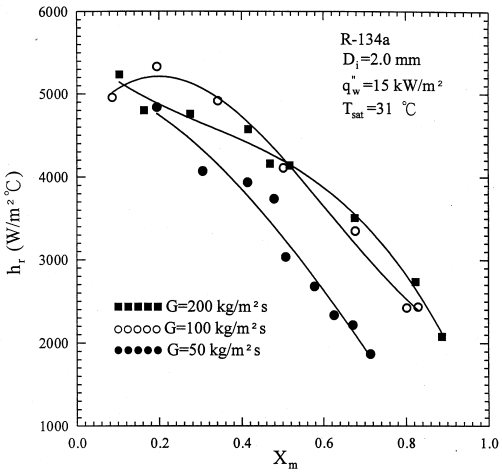

Fig. 8. Changes of the evaporation heat transfer coefficient with the mass flux at a higher imposed heat flux of $q''_w = 15$ kW m^{-2} for $T_{sat} = 31^{\circ}C$.

for $G = 100$ kg m^{-2} s^{-1}. It is of interest to note that at $G = 200$ kg m^{-2} s^{-1} and $q''_w = 5$ kW m^{-2} an increase in the vapor quality causes an increase in the heat transfer. But for other cases in Figs 7 and 8, the evaporation heat transfer deteriorates at increasing vapor quality except for $X_m < 0.25$. At the high imposed heat flux Fig. 8 shows that the evaporation heat transfer does not always rise with the mass flux especially when G is raised from 100 to 200 kg m^{-2} s^{-1}.

Finally, it is necessary to compare the present data for the R-134a evaporation heat transfer in a small pipe to those in large pipes reported in the literature. Due to the limited availability of the data for large pipes with the same ranges of the parameters covered in the present

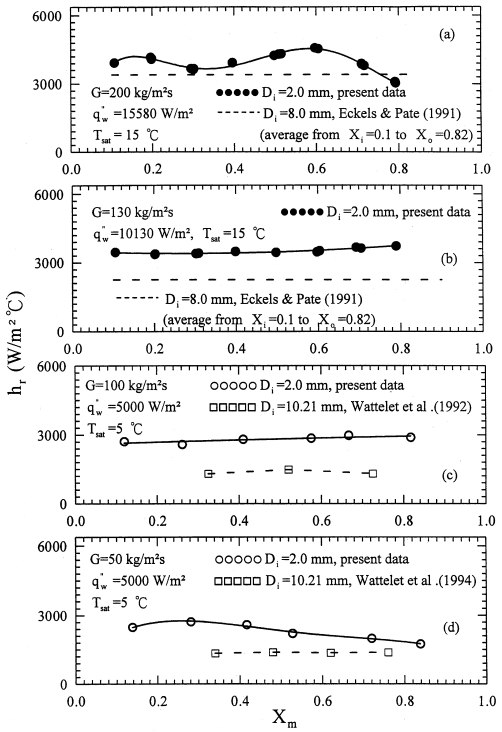

Fig. 9. Comparison of the present heat transfer data with those for the larger pipes [2, 6, 15].

study the comparison is only possible for a few cases. This is shown in Fig. 9, in which our data are compared with those from Eckels and Pate [2] and Wattelet et al. [6, 15]. Note that the data from Eckels and Pate [2] are average h_r values measured in a long pipe of 3.67 m in length with the vapor quality varying from 0.1 at the pipe inlet to 0.82 at the exit. The results in Fig. 9(a) manifest that at a high mass flux of 200 kg m^{-2} s^{-1} the R-134a evaporation heat transfer coefficient for the small pipe is about 10–30% higher than that for the large pipe with $D_i = 8.0$ mm for $X_m < 0.7$. But at $X_m > 0.75$ the opposite is the case. At lower G of 130 and 100 kg m^{-2} s^{-1} the evaporation heat transfer in the small pipe is substantially better than that in the large pipes (Figs 9(b), (c)) over the entire range of the vapor quality tested in the present study. At an even lower G of 50 kg m^{-2} s^{-1} the heat transfer coefficient associated wit the evaporation of R-134a in the small pipe (Fig. 9(d)) is still better. But at a high vapor quality $X_m > 0.7$ the heat transfer coefficients in the small and large pipes are rather close.

4.2. Two-phase frictional pressure drop

The frictional pressure drops associated with the R-134a evaporation in the small pipe under various flow

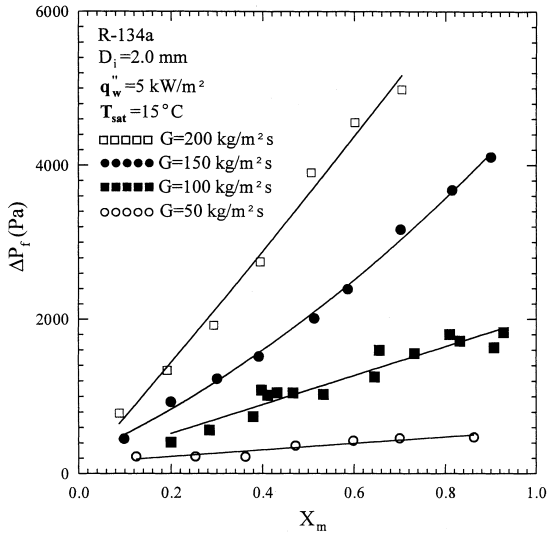

Fig. 10. Frictional pressure drop variations with the mean vapor quality at various mass fluxes for $T_{sat} = 15°C$ and $q''_w = 5$ kW m^{-2}.

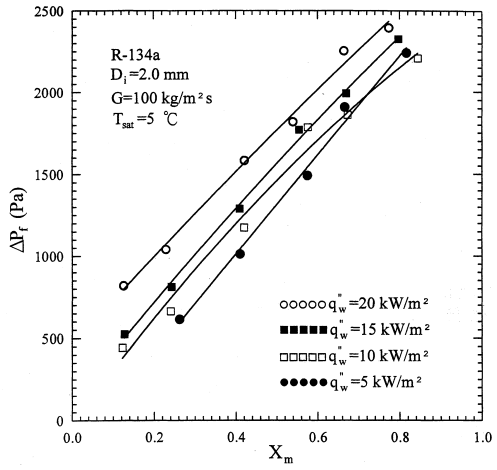

Fig. 11. Frictional pressure drop variations with the mean vapor quality at various wall heat fluxes for $T_{sat} = 5°C$ and $G = 100$ kg m^{-2} s^{-1}.

and thermal conditions are presented in Figs 10–12. The results in Fig. 10 for various mass fluxes indicate that at a given mass flux the pressure drop is larger for a higher vapor quality. This pressure drop increase with the quality is more pronounced for a higher mass flux. It is important to note that at a given vapor quality the pressure drop monotonically increases with the mass flux. This simple trend is very different from the complicate variation of the evaporation heat transfer coefficient with the mass flux examined in Figs 7 and 8. Moreover, Fig. 11

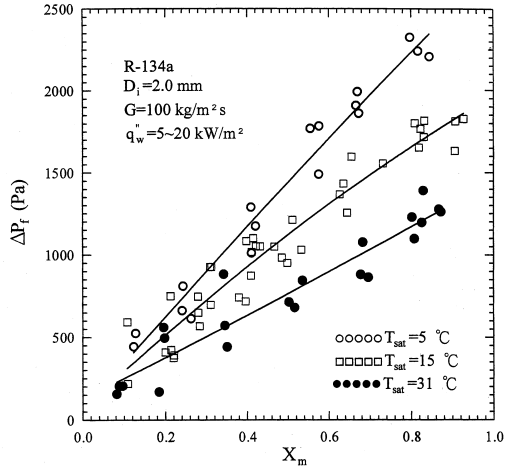

Fig. 12. Frictional pressure drop variation with the mean vapor quality at various refrigerant saturated temperatures for $G = 100$ kg m^{-2} s^{-1} and $q''_w = 5$–20 kW m^{-2}.

suggests that an increase in the imposed wall heat flux results in a mild increase of the pressure drop except at a high vapor quality ($X_m > 0.7$) and the variation is also simple, unlike those in Figs 4 and 5 for the change of the evaporation heat transfer with the wall heat flux. We further note that the effect of the saturated temperature change on the pressure drop can be significant at a high quality ($X_m > 0.65$), as shown in Fig. 12. More specifically, for a higher T_{sat} the pressure drop is lower. It is worth mentioning that the saturated temperature has been shown to exhibit profound effects on the evaporation heat transfer (Fig. 6).

4.3. Correlation equations

Correlation equations for the heat transfer coefficient and friction factor associated with the R-134a evaporation in the small pipe considered here are important in the future practical thermal design of the evaporators in various air conditioning and refrigeration systems. Based on the present data, a heat transfer correlation similar to that proposed by Kandlikar [16] is found to be suitable. The correlation is

$$h_{tp} = (C_1 C_o^{C_2} + C_3 B_o^{C_4} Fr_{lo})(1 - X_m)^{0.8} h_l \quad (17)$$

where h_l is the all liquid, laminar fully developed convection heat transfer coefficient and is assumed to be equal to 4.364 D_i/k_l. Three non-dimensional groups are included in the above equation, the convection number C_o, boiling number B_o and all liquid Froude number Fr_{lo}. They are defined as

$$C_o \equiv \left(\frac{1 - X_m}{X_m}\right)^{0.8} \left(\frac{\rho_g}{\rho_l}\right)^{0.5} \quad (18)$$

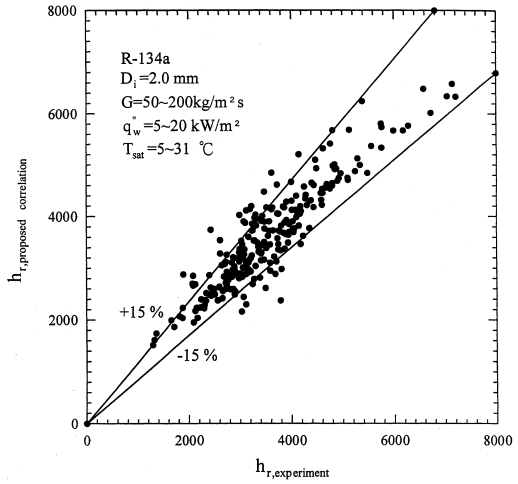

Fig. 13. Comparison of the proposed heat transfer correlation with the measured data.

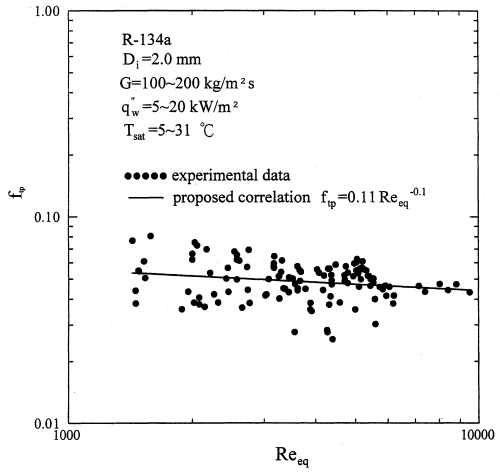

Fig. 14. Variations of the measured two phase friction factor with the equivalent Reynolds number and compared with the proposed correlation.

$$B_o \equiv \frac{q''_w}{i_{fg} G} \tag{19}$$

and

$$Fr_{lo} \equiv \frac{G^2}{(\rho_l^2 g D_i)}. \tag{20}$$

The empirical constants C_1, C_2, C_3 and C_4 are assumed to be function of the all liquid Reynolds number Re_l and reduced temperature T_R. They can be expressed as

$$C_m \equiv C_{m,1} Re_l^{C_{m,2}} T_R^{C_{m,3}} \tag{21}$$

where $m = 1$, 2, 3 and 4. The best fitting values for the constants $C_{m,1}$, $C_{m,2}$ and $C_{m,3}$ are listed in Table 2. Figure 13 shows that more than 80% of the data measured in the present study fall within $\pm 15\%$ of the above correlation (equation (17)).

Based on the present data of the friction factor shown in Fig. 14, an empirical correlation is proposed and it is

$$f_{tp} = 0.11 Re_{eq}^{-0.1} \tag{22}$$

where Re_{eq} is the equivalent Reynolds number proposed by Akers et al. [17],

$$Re_{eq} = \frac{G D_i}{\mu_l}\left[(1 - X_m) + X_m \left(\frac{\rho_l}{\rho_g}\right)^{0.5}\right]. \tag{23}$$

The average deviation between the present data and the proposed correlation is about 17%.

5. Concluding remarks

An experiment has been carried out in the present study to measure the heat transfer coefficient and pressure drop for the evaporation of R-134a flowing in a small pipe of 2 mm in diameter. The present results are quite

Table 2
Values of the constants in equation (21)

$C_m = C_{m,1} Re_l^{C_{m,2}} T_r^{C_{m,3}}$	$C_o > 0.5$			$0.15 < C_o \leqslant 0.5$			$C_o \leqslant 0.15$		
m	$C_{m,1}$	$C_{m,2}$	$C_{m,3}$	$C_{m,1}$	$C_{m,2}$	$C_{m,3}$	$C_{m,1}$	$C_{m,2}$	$C_{m,3}$
1	933.6	0.07575	26.19	47.3	0.3784	14.67	356600	−0.6043	18.59
2	−0.2	0	0	2612.8	0	37.270	1409.1	−0.5506	16.303
3	41700	0.5731	34.98	100150	0	24.371	12.651	0.3257	10.118
4	14.84	−0.0224	13.22	3.990	−0.1937	4.794	0.15	0	0

different from those for larger pipes and are summarized here. For a higher imposed wall heat flux the evaporation heat transfer coefficient is higher except in the high vapor quality region. The reverse is the case in the high vapor quality region for a high imposed wall heat flux. For most cases the heat transfer coefficient is higher at a higher saturated temperature of the refrigerant. The mass flux exhibits different effects at different vapor qualities and imposed wall heat fluxes. At a low imposed wall heat flux the heat transfer significantly increases for a small rise in the mass flux. But at a higher wall heat flux the increase in the heat transfer can be slight and even reduced. The effect of the mass flux on the pressure drop is rather simple with a higher ΔP_f for a rise in the mass flux. Moreover, a higher imposed heat flux usually results in a higher pressure drop. Finally, we noted that to some degree the evaporation heat transfer in the small pipe is more effective than that in larger pipes. For practical application empirical correlations were also proposed to correlate the present data for the heat transfer coefficient and friction factor in the small pipe.

During the course of this investigation it was realized that design of more compact and effective condensers is also important in improving the thermal efficiency of various refrigeration and air conditioning systems. Thus, an extension of the present study to the condensation of R-134a in small pipes is needed and will be explored in the near future.

Acknowledgements

The financial support of this study by the engineering division of National Science Council of Taiwan, R.O.C. through the contract NSC85-2221-E-009-046 and Dr B.C. Yang's help during construction of the present experimental facility are greatly appreciated.

References

[1] J.R. Thome, Boiling of new refrigerants: a state-of-the art review, Int. J. Refrig. 19 (1996) 435–457.
[2] S.J. Eckels, M.B. Pate, An experimental comparison of evaporation and condensation heat transfer coefficients for HFC-134a and CFC-12, Int. J. Refrig. 14 (1991) 70–77.
[3] S.J. Eckels, M.B. Pate, Evaporation and condensation of HFC-134a and CFC-12 in a smooth tube and a micro-fin tube, ASHRAE Transaction 97 (1991) 71–81.
[4] K. Torikoshi, T. Ebisu, Heat transfer and pressure drop characteristics of R-134a, R-32, and a mixture of R-32/R-134a inside a horizontal tube, ASHRAE Transactions 99 (1993) 90–96.
[5] K. Hambraeus, Heat transfer coefficient during two-phase flow boiling of HFC-134a, Int. J. Refrig. 14 (1991) 357–362.
[6] J.P. Wattelet, J.C. Chato, A.L. Souza, B.R. Christoffersen, Evaporation characteristics of R-12, R-134a, and a mixture at low fluxes, ASHRAE Transactions 100 (1994) 603–615.
[7] S.M. Sami, T.N. Duong, Two phase boiling characteristics of R-134a and R-12 in annuli of enhanced surface tubing, Int. Comm. Heat Mass Transfer 19 (1992) 203–214.
[8] A. Singh, M.M. Ohadi, S. Dessiatoun, Flow boiling heat transfer coefficients of R-134a in a microfin tube, J. of Heat Transfer 118 (1996) 497–499.
[9] X. Liu, Condensing and evaporating heat transfer and pressure drop characteristics of HFC-134a and HCFC-22, J. of Heat Transfer 119 (1997) 158–163.
[10] J.G. Collier, Convective Boiling and Condensation. 2nd Edition. McGraw-Hill International Book Company, 1981, pp. 26–108.
[11] S.M. Zivi, Estimation of steady steam void-fraction by means of principle of minimum entropy production, J. of Heat Transfer 86 (1964) 237–252.
[12] S.J. Kline, F.A. McClintock, Describing uncertainties in single-sample experiments, Mech. Eng. 75 (1953) 3–12.
[13] D.S. Jung, M. McLinden, R. Radermacher, D. Didion, Horizontal flow boiling heat transfer experiments with a mixture of R22/R114, Int. J. Heat and Mass Transfer 32 (1989) 131–145.
[14] M.G. Cooper, Flow boiling—the apparently nucleate regime, Int. J. Heat and Mass Transfer 32 (1989) 459–464.
[15] J.P. Wattelet, J.M. Saiz Jabardo, J.C. Chato, J.S. Panek, A.L. Souza, Experimental evaluation of convective boiling of refrigerants HFC-134a and CFC-12, ASME HTD-197 (1992) 121–127.
[16] S.G. Kandlikar, A general correlation for saturated two-phase flow boiling heat transfer inside horizontal and vertical tubes, J. of Heat Transfer 112 (1990) 219–228.
[17] W.W. Akers, H.A. Deans, O.K. Crosser, Condensation heat transfer within horizontal tubes, Chem. Eng. Prog. Symposium Ser. 55 (1959) 171–176.